

Effects of topography on facies and compositional zonation in caldera-related ignimbrites

GREG A. VALENTINE *Geoanalysis Group, M.S. F665, Los Alamos National Laboratory, Los Alamos, New Mexico 87545*

KENNETH H. WOHLTZ *Geology-Geochemistry Group, M.S. D462, Los Alamos National Laboratory, Los Alamos, New Mexico 87545*

SUSAN W. KIEFFER *Department of Geology, Arizona State University, Tempe, Arizona 85287*

ABSTRACT

Large-scale fluid dynamical processes during explosive eruptions within calderas are examined numerically by solving the full set of two-phase hydrodynamic equations with a topographic barrier, representing the rim of a caldera. The effect of the caldera rim on eruption dynamics depends on the relative locations of the rim and the impact zone where tephra collapsing from the eruption column strikes the ground. The distance of the impact zone from the vent is proportional to the collapse (fountain) height of the eruption column. Three significantly different eruption patterns have been observed in the simulations: (1) If the impact zone is outside the caldera rim, relatively continuous pyroclastic flow occurs outside the caldera. (2) If the impact zone is on or near the caldera rim, an initial pyroclastic current flows out of the caldera and is followed by a lapse in outflow during which the caldera fills up with ash. (3) If the impact zone is inside the rim, all initial pyroclastic flows are contained within the caldera unless the flows have sufficiently high initial densities and velocities to carry them over the rim. In most cases, recirculation of pyroclasts into the base of the column causes fountain height to decrease dramatically with time due to the "choking" effect of the ash. This recycling of ash in turn reduces the ability of pyroclastic flows to surmount the rim. The numerical models suggest several processes that cause the formation of multiple cooling and flow units in deposits outside a caldera from a single eruption of steady discharge. Compositional gaps may occur in outflow ignimbrite due entirely to interaction of eruption and emplacement dynamics with topography; sharp compositional gradients within a magma chamber are not necessarily implied by compositional gaps in outflow units. Outflow and intracaldera facies tuffs from the same eruptions can show different cooling histories and compositional variations because of these large-scale fluid dynamical processes.

INTRODUCTION

Calderas and caldera-related deposits have been important topics of geologic study for several decades because they commonly host economic grade ore and geothermal reserves, and because they represent "snapshot" sampling of magma reservoirs (for example, Hildreth, 1981) or direct sampling of the products of lower-crustal melting events (Francis and others, 1989). The relationships between outflow and intracaldera facies, and the overprint of eruption dynamics on original compositional variations in the magma must be understood for these applications.

Field observations of deposits and structures associated with caldera-forming eruptions suggest that many of these eruptions can occur from a vent or vents within a depression formed by syneruptive caldera collapse (Lipman, 1976, 1984; Elston, 1984). The depression may also be a pre-eruptive feature, as in systems of nested or coalesced calderas, such as the Valles-Toledo complex (Self and others, 1986; Heiken and others, 1986), the San Juan Mountains in Colorado (Steven and Lipman, 1976), the Timber Mountain-Oasis Valley complex in southern Nevada (Broxton and others, 1989; Warren and others, 1989), and the Taupo volcanic zone in New Zealand (Wilson and others, 1984).

Many silicic magma chambers are compositionally zoned (Trial and Spera, 1990). Interpretation of pyroclastic deposits is commonly based upon the assumption that there is a direct correspondence between the magma chamber and the deposits such that early-erupted (stratigraphically lower) deposits are tapped from the top of a chamber, and later-erupted deposits originate progressively deeper in the chamber. The presumption often associated with this interpretive scheme is that the parent magma is vertically zoned in a simple manner such that it is hotter and more mafic with increasing depth, either by a smooth or stepped gradient.

Some pyroclastic deposits show convincing petrological and geochemical evidence that this simple vertical zonation, and the straightforward correlation between ignimbrite zonation and that of the parent magma chamber, is in fact true (Fridrich and Mahood, 1987). Several processes, however, can complicate and obscure the original chamber zonation (Marsh, 1989; Trial and Spera, 1990): (1) the likely presence of significant lateral variations in magma chamber composition (Oldenburg and others, 1989); (2) magma withdrawal processes (Spera and others, 1986; Blake and Ivey, 1986); (3) viscosity segregation within the volcanic conduit (Carrigan and Eichelberger, 1990); (4) changes in vent structure and location, such as the transition from central-vent to ring-fracture eruption (Druitt and Sparks, 1985); (5) large-scale eruption dynamics, the topic of this paper; (6) the detailed emplacement mechanism of a deposit (layer by layer deposition producing vertical zonation, and *en masse* deposition producing lateral zonation); and (7) the possibility that pumice constituents in pyroclastic flows represent specific portions of chambers, whereas the finer ground mass constituents may represent other parts of the chamber (Warren and others, 1989). All of these processes can affect the final zonation that is observed in a pyroclastic deposit and must be considered in order to use eruption dynamics as an effective sampling tool to reconstruct the pre-eruptive magmatic state.

The effects of topographic barriers such as caldera rims also may control the lateral extent of early- versus later-erupted materials. In a review of some of the relations between outflow and intracaldera facies

tuffs, Lipman (1984) pointed out that the outflow-facies ignimbrite may consist of many cooling and flow units (a "compound" cooling unit; Smith, 1960), whereas the intracaldera facies is a simple cooling unit. Similarly, the compositional zonation patterns observed within the two facies commonly overlap to some degree but also have substantial differences (Lipman, 1984). Here we examine these issues using the results of two-dimensional numerical simulations.

APPROACH

The approach is based upon explicit numerical solutions of the equations of conservation of mass, momentum, and energy (Harlow and Amsden, 1975; Wohletz and others, 1984; Valentine and Wohletz, 1989a, 1989b; Wohletz and Valentine, 1990). The erupting fluid is a two-component mixture of gas and dispersed particles (ash). The gas is described by the ideal gas equation of state. Material properties used in these simulations can be found in Valentine and Wohletz (1989a). The conservation equations of ash and gas are calculated independently, so that they may have different temperatures, velocities, and volume fractions, but they interact with each other by drag forces and heat transfer. The governing

equations form a system of 8 partial differential equations and 8 algebraic equations with 16 dependent variables. The partial differential equations are approximated by finite difference methods and solved on a large computer. The runs reported in this paper each required 2 to 10 hours of cpu time on a Cray X-MP.

Hot ash and gas in specified proportions and flow conditions enter the computational domain (Fig. 1) beginning at time $t = 0.0$. The atmosphere in the domain is initially isothermal at 300 °K, and pressure and density decrease exponentially with height. Because we assume cylindrical symmetry, we calculate only a half-space; the symmetry axis is defined as a reflecting boundary. The top and right-hand boundaries are open to allow material to flow out of the domain. The bottom boundary is treated as a frictionless substrate, for convenience, although a better approximation would be a no-slip reflector because of basal shear. Practical limits require a mesh size of the order of 100 m by 100 m, however, and therefore the boundary layer cannot be resolved. Boundary-layer processes in similar high-velocity volcanic flows occur at the scale of a few centimeters to a few tens of meters (Kieffer and Sturtevant, 1988). We emphasize that outcrop-scale features (centimeters to tens of meters) are not resolved with this mesh size. The calculations are relevant only for the large-scale dynamics of the eruptions.

A caldera rim is simulated by adding a rectangular block to the bottom boundary to represent the volcanic highlands that commonly surround calderas (see Fig. 1). Because of the cylindrical symmetry of the system, the block models an annular obstacle, or caldera rim, around the vent. We discuss the limitations of this approximation at the end of the paper. This annular rim, like the rest of the bottom boundary, is defined as

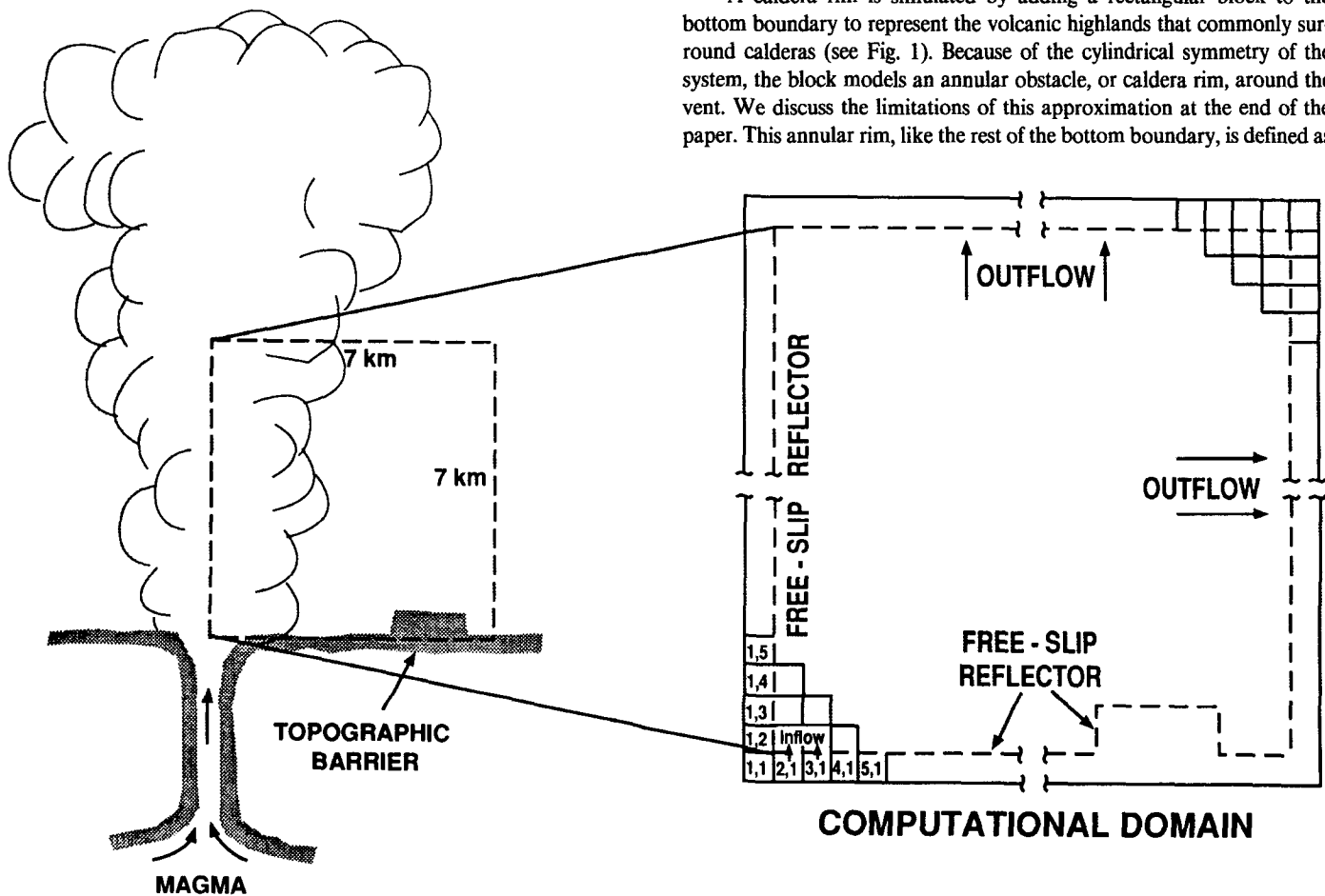


Figure 1. The computational domain and boundary conditions. The domain is 7 km \times 7 km, and is divided into a grid of 100 m \times 100 m finite difference cells. The bottom and left boundaries are free-slip reflectors, where velocities perpendicular to the boundaries are set to zero, but velocities parallel to the boundaries are determined by the interior flow. The left boundary is the symmetry axis in cylindrical coordinates. The top and right boundaries allow outflow by setting all variables equal to their values just inside the boundaries. The raised block on the bottom boundary illustrates the representation of caldera rims used in the calculations.

TABLE 1. EXIT CONDITIONS AND CALDERA RIM (OBSTACLE) SPECIFICATIONS FOR MODEL ERUPTIONS

Run	Exit velocity (m/s)	Weight % H ₂ O	Exit pressure (MPa)	Vent radius (m)	Pyroclast radius (m)	Discharge rate (kg/s)	Obstacle dimensions height (m) × width (m)	Obstacle location (m from vent center)
105	300	0.74	0.1	200	10 ⁻⁴	9.1 × 10 ⁸	500 × 1,500	4,000
107	300	0.74	0.1	200	10 ⁻²	9.1 × 10 ⁸	500 × 1,500	4,000
108	370	2.50	0.1	400	10 ⁻³	1.3 × 10 ⁹	500 × 1,500	4,000
109	265	1.40	0.1	400	10 ⁻³	1.8 × 10 ⁹	500 × 1,500	4,000
110	300	0.74	0.1	200	10 ⁻⁴	9.1 × 10 ⁸	500 × 1,000	1,800
111	265	1.40	0.1	400	10 ⁻³	1.8 × 10 ⁹	200 × 1,500	4,000
112	300	4.88	0.69	200	10 ⁻¹	9.5 × 10 ⁸	500 × 1,000	3,000
113	300	4.88	0.69	200	10 ⁻¹	9.5 × 10 ⁸	300 × 1,000	3,000
117	290	1.70	0.1	200	10 ⁻⁴	4.6 × 10 ⁸	-	-
118	290	1.70	0.1	200	10 ⁻⁴	4.6 × 10 ⁸	500 × 1,000	2,900
119	290	1.70	0.1	200	10 ⁻⁴	4.6 × 10 ⁸	500 × 1,000	5,100
120	290	1.70	0.1	200	10 ⁻⁴	4.6 × 10 ⁸	500 × 1,000	1,100

Note: exit temperature for all simulations is 1200° K, material density of particles is 2400 kg/m³.

a free-slip obstacle. Thus the effects of the obstacle on the flows are due purely to the conversion of kinetic energy to potential energy and the pressure changes that accompany flow up and over the rim (commonly referred to as "form drag"); friction drag is not simulated. The location and dimensions of the annular rim were varied in a manner that allowed us to study its effects on eruption dynamics but were kept within geologically reasonable values. For example, in our first runs, we placed the leading edge of the rim at 4.0 km from vent and gave it dimensions of 0.5 km high by 1.5 km wide. These values are similar to the size and location of the rim (relative to the inferred ring vent position) of the Valles caldera rim during the most recent eruption of Bandelier Tuff (Smith and others, 1970; Wohletz and others, 1984).

Many natural caldera eruptions involve eruption from ring vents, rather than from a central vent as modeled here. The general processes (at a qualitative level) associated with eruptions from ring vents can be expected to be similar to those of central vent eruptions because in both cases the pyroclastic flows experience radial divergence as they travel away from their sources.

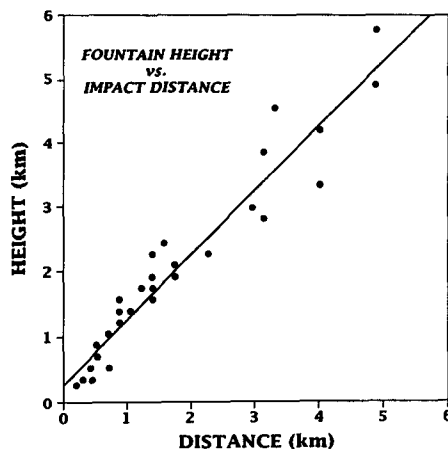


Figure 2. Initial fountain height versus impact distance from vent. Points represent the flow stagnation locations for numerical simulations discussed by Valentine and Wohletz (1989a). Note that this plot shows only the values during the initial phase of fountain formation; in any given simulation, the fountain height and impact distance continue to evolve throughout the simulation. The impact distance for eruptions of multiple particle sizes could be spread over a range, such that discrete stagnation points would not exist.

SIMULATIONS AND RESULTS

The numerical experiments reveal three main classes of behavior for pyroclastic fountain eruptions within calderas, depending upon whether the rim is outside, coincidental with, or inside the location of impact of pyroclasts falling from the fountain. The exit conditions and caldera-rim specifications for the simulations discussed are given in Table 1.

Fountain Height versus Impact Distance Relationship

Analyses of ~30 numerical fountain experiments without caldera rims (Fig. 2; experiments originally reported in Valentine and Wohletz, 1989) suggest that in most cases the ejecta in a negatively buoyant eruption fall to the ground some distance from the vent (the "impact distance") that is equal to the initial fountain height minus a few hundred meters. In detail the dynamics of compressible, two-phase fountains involve interplay between exit pressure and particle settling velocity as well as exit velocity, vent radius, and gas content (Valentine and Wohletz, 1989a; see also review by Woods, 1988). The scatter of points in Figure 2 is due to variations in these factors, which influence both fountain height and impact distance. For example, holding all other factors constant, the ratio of impact distance to fountain height will be reduced by an increase in particle size.

The fountain height versus impact distance relationship is important for understanding the possible effects of a caldera rim on a given eruption. For an eruption with a given fountain height, if the distance to the caldera rim lies to the right of the best-fit line in Figure 2, then impact occurs within the caldera. Conversely, if the distance to the rim lies to the left of the best-fit line, then impact will occur outside the caldera.

Eruption with No Topographic Barrier

For reference, we begin by briefly discussing a pyroclastic fountain eruption over a flat ground surface (Fig. 3); see Valentine and Wohletz (1989a, 1989b) for details. The combination of exit parameters for this numerical eruption was determined from the theory of Wilson and others (1980).

Initially a jet moves upward from the vent to an elevation of about 3.5 km. The head of the jet is relatively wide compared to the body of the jet because a vortex structure develops due to penetration into the atmosphere; this structure is referred to as the *working surface*. The body of the jet widens as it flows due to turbulent diffusion into the clean atmosphere; conversely, this involves diffusion, or in a crude sense, entrainment, of clean atmosphere into the ash-laden jet. At 3.5-km elevation (the initial

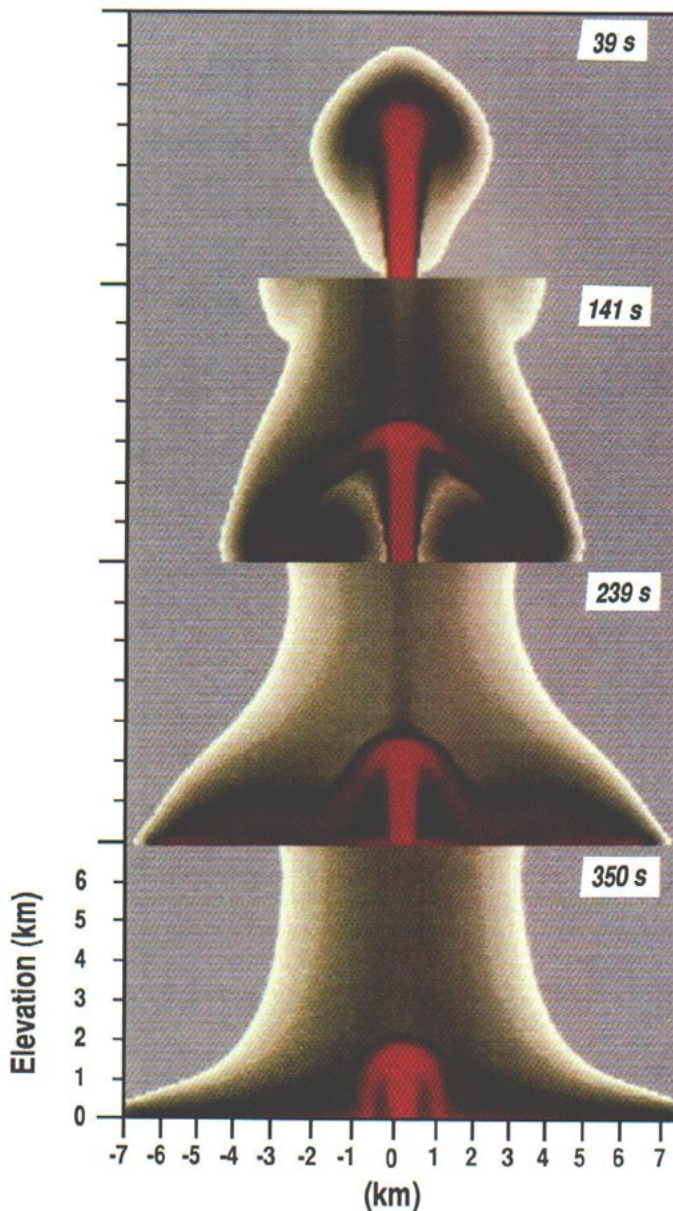


Figure 3. Snapshots of an eruption with a flat ground surface (run 117, Table 1). (a) through (d) are snapshots at $t = 39$, 141, 239, and 350 s after eruption initiation, respectively. The variable shown is ash-volume concentration; red is high concentration; decreasing concentration progresses from black to light gray. Maximum concentration is $\sim 10^{-3}$; minimum is 10^{-9} .

fountain height), the initial kinetic energy of the jet at the vent has been converted to potential energy and also dissipated by drag on the atmosphere (Fig. 4). As the upward flow decelerates, a zone of high pressure forms due to stagnation, and material begins to spread laterally. Because this laterally spreading mixture of gas and ash is denser than the atmosphere, it begins to fall, eventually impacting the ground at a distance of about 3 km from the center of the vent. The collapsing part of the fountain (the *stem*) in this simulation initially spreads laterally faster than it falls because the mixture density at the top of the fountain is only slightly

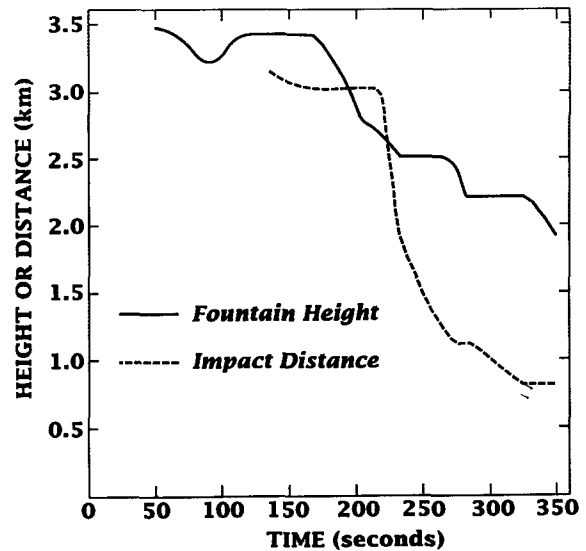


Figure 4. Evolution of fountain height and impact distance with time for run 117 (see Fig. 3). Initially the column collapses at an elevation of 3.5 km beginning at $t = 50$ s after the eruption discharge begins. Approximately 80 s later, the collapsing mixture impacts the ground at about 3.2 km from the vent. Pyroclastic flows move outward, away from the vent, and inward, toward the vent. 40 s later ($t = 170$ s), the inward-moving pyroclastic flow has reached the vent, causing some “choking” of the fountain so that its height rapidly decreases to about 2.5 km over a period of about 60 s. The decreasing fountain height in turn leads to decreasing impact distance. Each step-like change in the fountain height or impact distance represents a temporary equilibrium between pulses of “choking” pyroclastic flow. This is especially apparent on animations of the simulations.

greater than the atmosphere. From this impact zone, the mixture forms pyroclastic flows that spread laterally along the ground, both away from the vent and back toward it as pyroclastic flows. Concurrently the fountain height decreases so that it is about 0.7 of the initial height, a feature predicted by Turner (1973). As the eruption evolves with time, the inwardly directed component of pyroclastic flow eventually reaches the vent and is reincorporated into the base of the eruption column, where it is accelerated upward. This upward acceleration extracts some upward momentum from the column, resulting in a gradual decrease in fountain height with time; because of this, the impact distance from the vent decreases with time (Fig. 4).

From this simulation, we suggest that in real central vent eruptions over relatively flat terrane the initial pyroclastic flow material will have higher mobility than later erupted material because it falls from the relatively high initial fountain (all other variables being constant). It follows that early pyroclastic flows will be the most likely to surmount an obstacle such as a caldera rim. The decreased fountain height and the shielding of the inner fountain from cool atmosphere, furthermore, lead to increasing temperature of the pyroclastic flows, a process which has been discussed in detail by Sparks and others (1978).

By $t = 250$ s, the outward-flowing component of pyroclastic flow has reached the right boundary of the computational domain and continues to flow out of the domain for the duration of the experiment. Throughout the development of the fountain, a low-concentration cloud of ash rises buoyantly above the fountain and pyroclastic flows; fallout from this type of

dynamics of the eruption are identical in the two cases until the outward-moving pyroclastic flow encounters the caldera rim. Except for a small amount of material that gets about half way over the rim, the pyroclastic flow does not have enough momentum to surmount the obstacle. The flow field at $t = 350$ s appears to have reached a relatively steady state, with pyroclasts gradually ponding within the caldera and a buoyant ash cloud continuously rising above the entire caldera. Although the simulation was not carried out to longer times, we expect that the eruption would continue in this manner until the caldera is filled with pyroclasts, after which pyroclastic flows would breach the rim and flow outward. For this type of eruption, there would be a significant time lag between the beginning of the eruption and the formation of outflow ignimbrite.

The simulation in Figure 5b exhibits a fountain behavior where larger particles prevent the collapsing portion from spreading laterally as far as the simulation in Figure 5a. Ash radial velocity (Fig. 6a) has a maximum velocity of 125 m/s, directed outward, at about 1.8 km from the vent for $t = 93$ s. Velocity decreases toward the vent, reaching zero at the impact point of the collapsing tephra. Between the impact point and the vent, velocities are negative, because pyroclasts flow toward the vent. Ash vol-

ume fraction gradually increases with time in the caldera as more ash is supplied and particles settle (Fig. 6b). Ash temperature has a more complex evolution (Fig. 6c), first increasing with time as hotter ash is supplied to the caldera, then decreasing in the outer parts of the caldera due to cooling and progressive isolation from the shrinking fountain. Gas pressure (Fig. 6d) shows two maxima. (1) Within about 1.5 km of the vent, a pressure maximum occurs that corresponds with the impact zone of the collapsing pyroclasts; the high pressure here is due to stagnation effects. Note that with increasing time this maximum migrates toward the vent due to the decrease in impact distance (correlating with the decrease in fountain height). (2) A second high-pressure zone exists at later times at the leading edge of the rim. This zone is also the result of a stagnation pressure where pyroclastic flow material impinges upon the rim and is brought to zero radial velocity.

Caldera Rim within the Impact Zone

In contrast to the previous results, when the fountain impact zone is outside the rim, extracaldera pyroclastic flows always develop. Snapshots

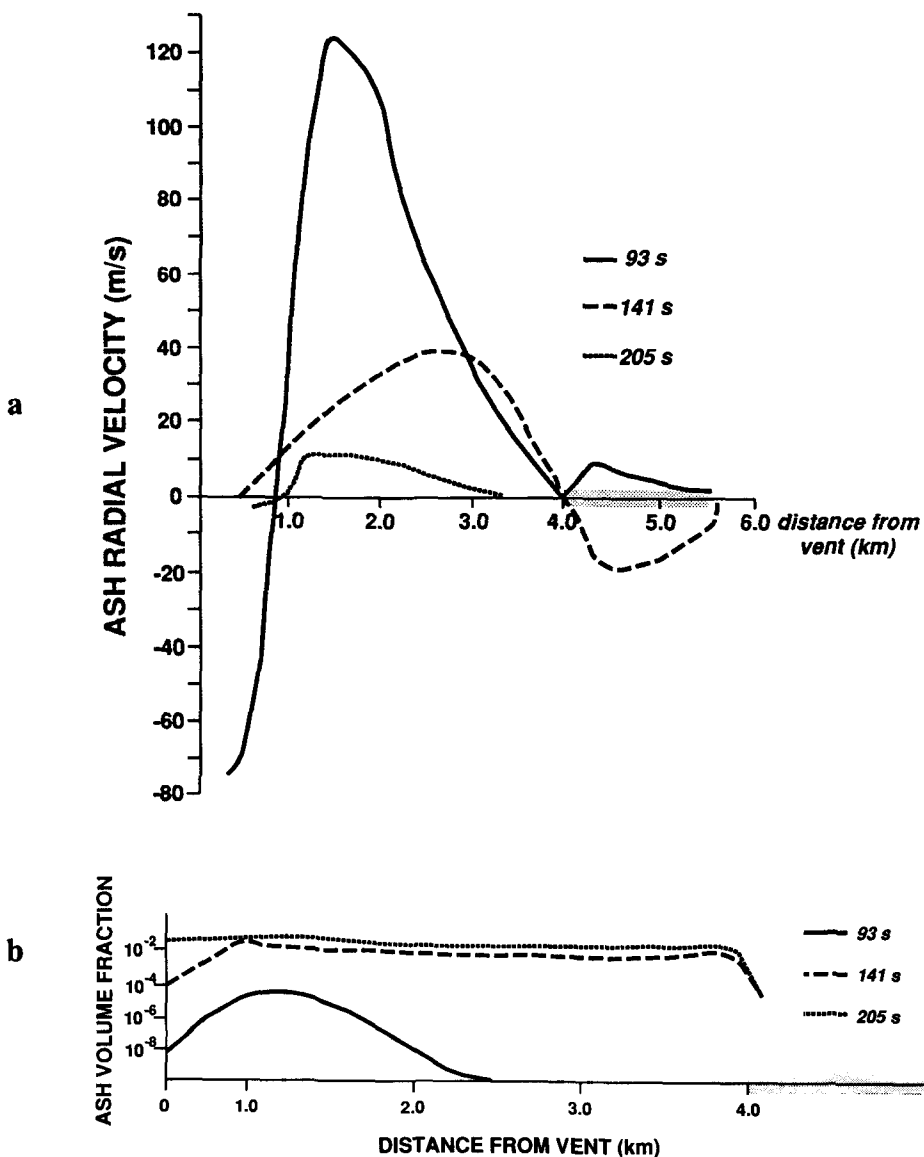


Figure 6. Radial variations along the ground surface for run 107 (see Fig. 5b), with location of caldera rim shown by shading. (a) Radial velocity of the ash, (b) ash volume fraction. (Continued on following page.)

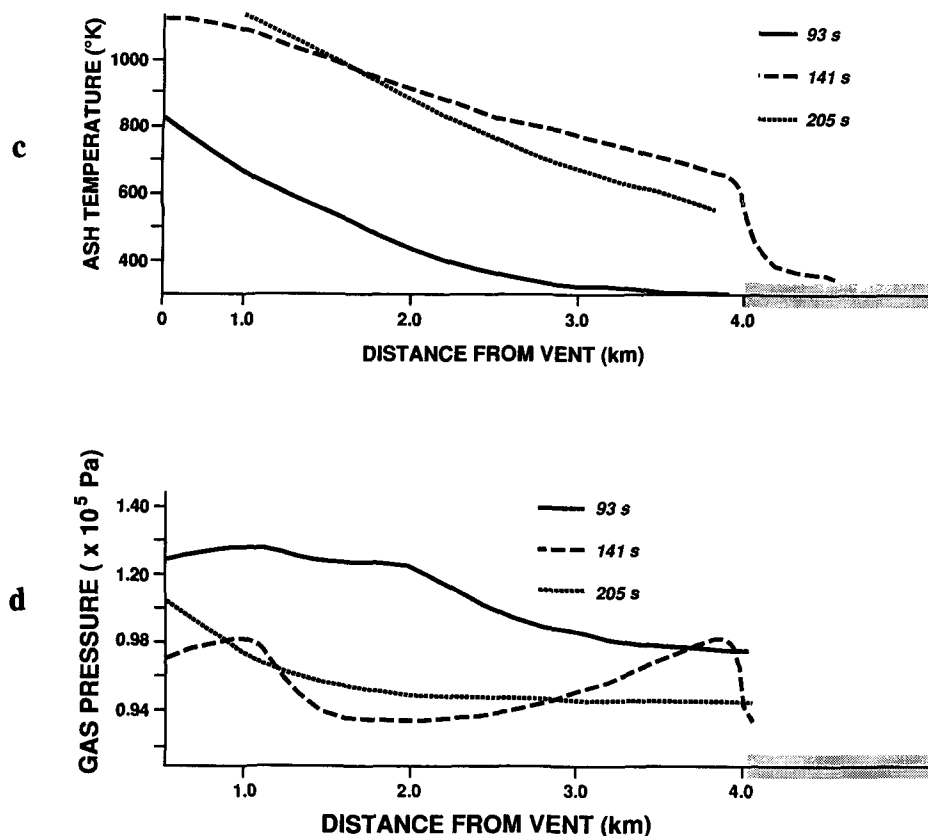


Figure 6. (Continued).
(c) Ash temperature (note that the minimum temperature for welding is about 800 °K), (d) gas pressure.

of a numerical eruption where the caldera rim is close to the vent and well inside the impact zone of the fountain are shown in Figure 7. The proximity of the caldera rim to the vent in this simulation has a direct effect on the development of the fountain. At early times, when the working surface of the eruption jet is still at low elevations, some ash is trapped along the ground by the rim instead of being recirculated upward with the rest of the working surface. The proximity of the rim also decreases the entrainment of clean atmosphere into the jet. Both effects cause the jet to have a higher density than it does if there is no rim or a relatively distant rim (compare with Figs. 3, 5a, and 8a). The fountain structure thus influenced by a rim has a narrower width than a fountain unconstrained by a rim because the collapsing mixture is relatively denser. The resulting pyroclastic flow produced by the fountain consists of two parts: (1) a relatively stagnant pond within the caldera and (2) a flow that begins at early times and spreads continuously outward. The outward-moving pyroclastic flow moves more slowly than that in Figure 3. This is due to the lower fountain height that results from the near-vent rim. We do not provide detailed profiles of variables for this simulation because the flow patterns are relatively simple. In this type of eruption, the outflow and intracaldera facies deposits are emplaced simultaneously.

Caldera Rim Coincidental with Impact Zone

In the previous two sections, we have discussed the end-member cases in which a distant rim causes full ponding of deposits within the caldera and a proximal rim allows a relatively continuous outflow sheet. The case where the collapsing pyroclast/gas mixture impacts directly upon the caldera rim is perhaps the most interesting of the cases discussed in this paper. High-energy initial pyroclastic flows can form outside the caldera

(as in the proximal-rim case), but later low-energy pyroclastic flows can be trapped within the caldera (as in the distal-rim case).

The first example of this type of eruption is illustrated in Figure 8a. When the collapsing mixture impacts the rim, some of it flows outward over the obstacle to form a pyroclastic flow that eventually falls to the ground and flows away from the rim to form outflow facies ignimbrite. Simultaneously, part of the collapsing mixture is diverted back toward the vent and begins to form intracaldera facies ignimbrite. As the eruption progresses, the proportion of material flowing out of the caldera decreases relative to that which is retained within the caldera because the fountain height decreases. Thus the intracaldera deposits would provide a relatively continuous record of the eruption, but the outflow facies may not, depending on the details of fountain height, rim dimensions, and outflow energy.

Another example of this type of eruption in which the initial pulse of outflow is more pronounced is depicted in Figure 8b. The collapsing mixture impacts the caldera rim at about $t = 120$ s. At this time, a pyroclastic current flows outward over the rim for a few hundred meters before it touches down outside the caldera. This current continues to travel away from the caldera, but it is eventually nearly disconnected from the main fountain as the fountain decreases in height. Within the caldera, high-concentration flows along the floor are blocked (Valentine, 1987) by the caldera wall, and intracaldera facies deposits begin to accumulate. It can be assumed that as the eruption progresses the caldera will fill until pyroclastic flows spill over the rim to once again produce outflow facies deposits. We did not carry the simulation out to the necessary time to verify this for practical reasons.

Radial variations of ash velocity, ash-volume fraction, ash temperature, and gas pressure along the ground surface for the eruption in Figure 8b are presented in Figure 9. Ash velocity reaches a maximum of about 80

Figure 8. Snapshots of two eruptions where the caldera rim is coincidental with the impact zone. (a) Run 118 at $t = 115, 176, 254,$ and 350 s; (b) run 112 at $t = 86, 124, 142,$ and 202 s. Same variable and color bar as in Figure 3.

the caldera rim, there will be a significant delay in outflow events because the caldera must fill up to allow pyroclastic flows to spill out. In this case, the intracaldera deposits would show the most complete range of compositional zonation and would be stratigraphically simple. The outflow facies would also be stratigraphically simple but would not preserve the initial compositions.

For cases where the impact zone is on the rim (lower row of Fig. 10), or where the impact is within the caldera but the initial pyroclastic flows have sufficient momentum to surmount the rim, the resulting deposits could potentially contain a very complex record which may not be easily inverted to give the initial magma chamber properties. Intracaldera facies

ignimbrite would deposit relatively continuously throughout the entire eruption and would thus show the full range in composition without stratigraphic breaks. Outside the caldera, initial pyroclastic flows would deposit some ignimbrite, but after this initial pulse, there would be a period of no outflow while the caldera fills. Only when the caldera is full would pyroclastic flows once again spill over the rim. These processes would produce an apparent compositional gap in the outflow deposits. The stratigraphy would show an initial relatively high-energy, low-temperature pyroclastic flow deposit or possibly a surge or a deposit that is transitional between the two. Such an eruption would form a flow unit which may have ash-cloud surge or fallout at its top due to the significant break in

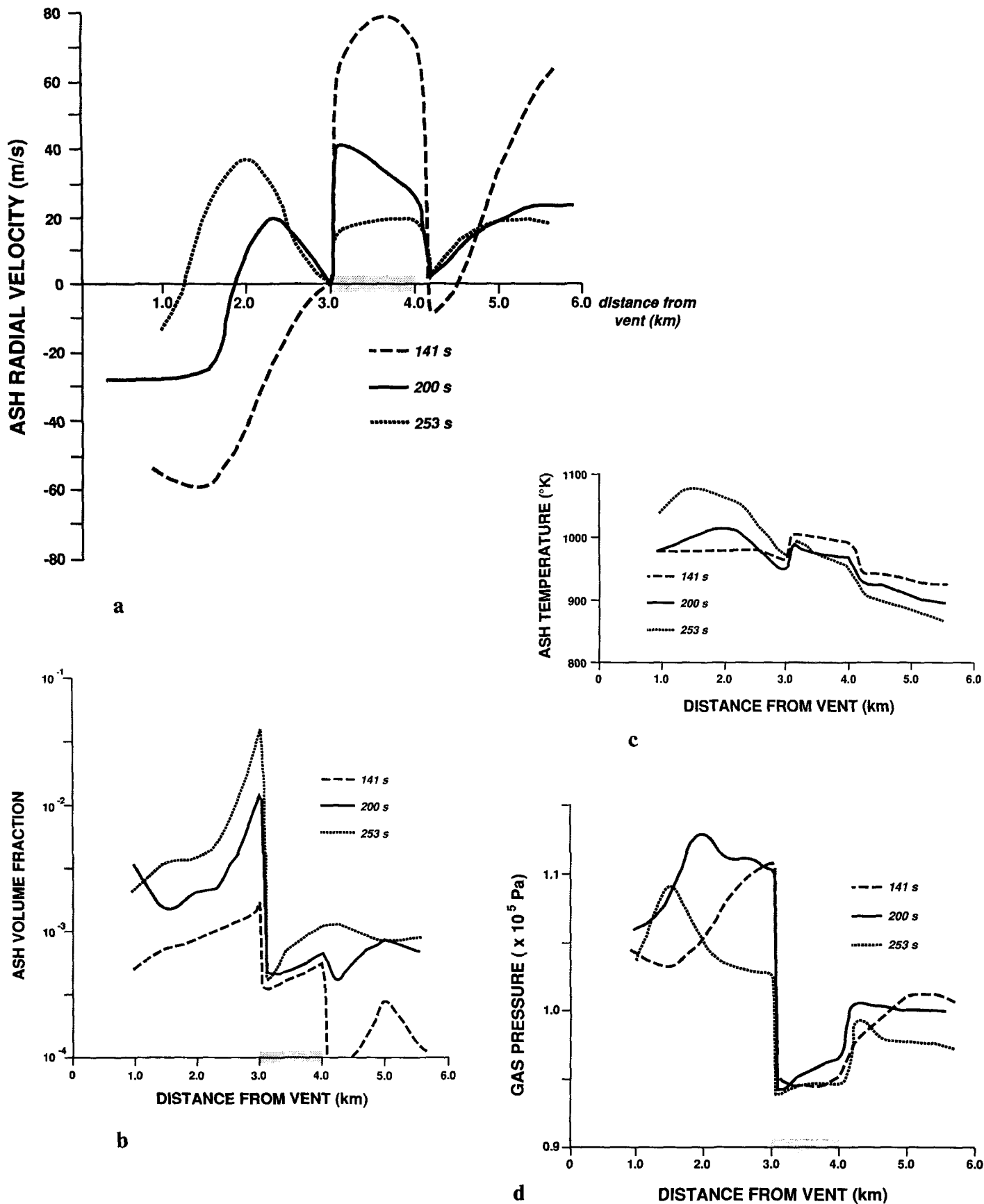


Figure 9. Radial variations along the ground surface for run 112 (see Fig. 8b), with location of caldera rim shown by shading. (a) Ash radial velocity, (b) ash-volume fraction, (c) ash temperature (again note that minimum welding temperature corresponds to ~ 800 °K), (d) gas pressure.

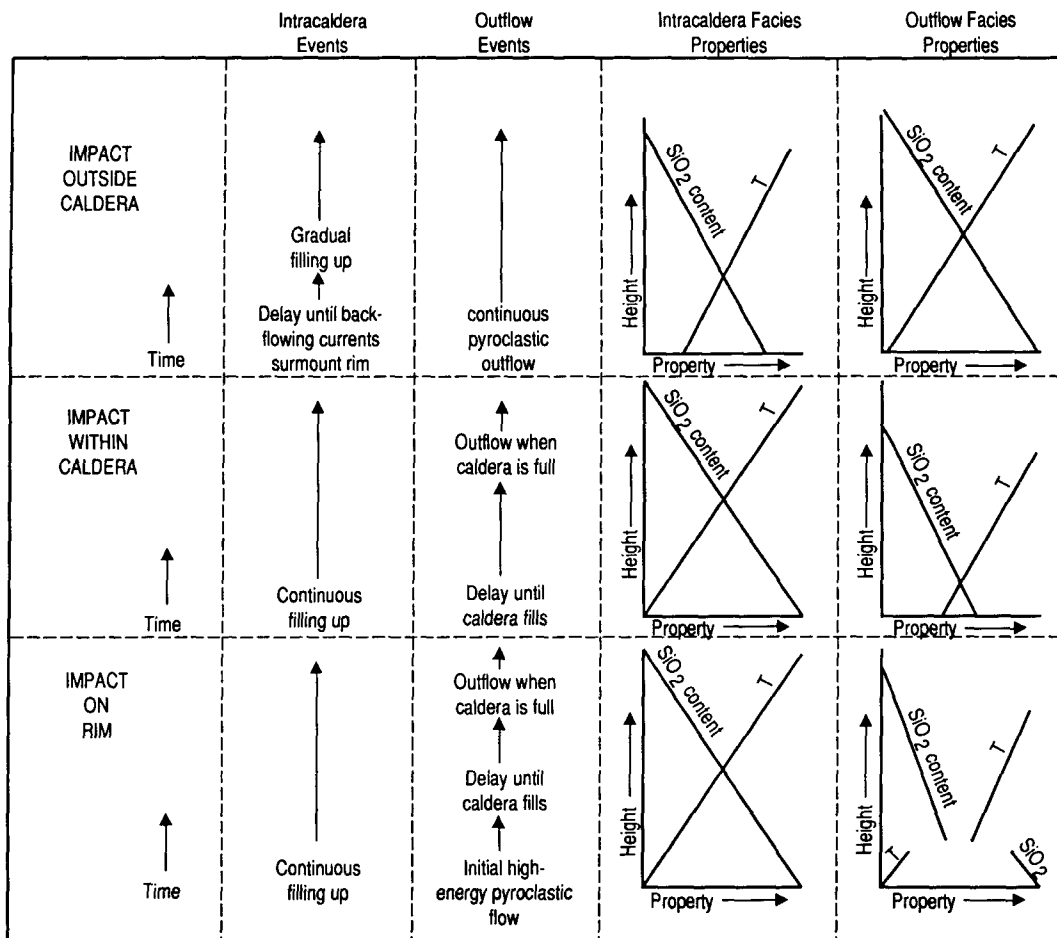


Figure 10. Conceptual illustration of events inside and outside a caldera, and the resulting variations in the deposits, for eruptions with the impact zone outside, within, and coincidental with the caldera rim. Two parameters, SiO₂ content and temperature (T), are shown as functions of stratigraphic height. For simplicity, it is assumed that the erupting magma becomes progressively more mafic and hotter with time in each eruption, and that the magma chamber is continuously zoned (that is, no compositional gaps).

time during caldera filling. The time break might also result in a cooling break. Above this break would be a higher-temperature, lower-energy, relatively mafic pyroclastic flow unit resulting from eventual caldera filling. These types of processes may explain field observations where outflow-facies ignimbrites show compound cooling units but correlative intracaldera facies form simple cooling units (Lipman, 1984).

More complex relationships can be envisioned by combining (*via* thought experiment) the above fluid-dynamic processes with some of the other structural processes that can occur during a caldera-forming eruption. For example, consider the complicated flow that could occur during an eruption where initially there is no topographic depression but the caldera collapses during the eruption. In this case, substantial outward-moving pyroclastic flows may occur during the initial phases of the eruption, but their apparent energy would decrease with time (stratigraphic height) as more of their initial energy is used in surmounting the developing rim. Eventually the barrier would be high enough that, combined with the decreasing fountain height, all outflow is stopped until the caldera fills. Another possibility is that during phases when most outflow is due to spilling out of a filled caldera, multiple flow units may form due to intermittent collapse events in the caldera. The caldera may fill and produce some outflow, but suddenly collapse, say, a few tens of meters, leading to a

break in outflow while new ash is added to the now deeper caldera. In this manner, multiple pyroclastic flow/cooling units could be generated in the outflow ignimbrite (but not necessarily in the intracaldera facies) even if the eruption discharge is steady. Implications of outflow versus intracaldera compositional zonation for timing of caldera collapse have been discussed by Lipman (1984).

The numerical simulations reported suggest that the full range of compositions for a given eruption is more likely to be found in the intracaldera-facies deposits than in outflow facies, except in cases where the impact zone is outside the caldera rim. Many of the variations with stratigraphic height in the outflow facies may be due to interaction among varying fountain height, flow/emplacement mechanisms, and the changing topography associated with a given caldera eruption. Major flow or cooling breaks in an intracaldera deposit are likely to reflect real breaks in the discharge and the magmatic processes at depth, whereas such breaks in the outflow may be related only to topographic effects.

ACKNOWLEDGMENTS

A video tape animation of some of the numerical eruptions discussed in the paper was prepared by Steve Hodson and Lynn MacDonald; it is

available upon request. Hodson and MacDonald are gratefully acknowledged for their contribution to graphic visualization for this study. This work was supported by the U.S. Department of Energy's Institutional Supported Research program at Los Alamos National Laboratory and by the U.S. Geological Survey. R. G. Warren, Wes Hildreth, and Armin Freundt provided thoughtful reviews. We thank C. F. Keller, Wes Myers, Sumner Barr, Ken Eggert, and Ruth Demuth for strong institutional and personal support.

REFERENCES CITED

- Blake, S., and Ivey, G. N., 1986, Magma-mixing and the dynamics of withdrawal from stratified reservoirs: *Journal of Volcanology and Geothermal Research*, v. 30, p. 153-178.
- Broxton, D. E., Warren, R. G., Byers, F. M., and Scott, R. B., 1989, Chemical and mineralogic trends within the Timber Mountain-Oasis Valley caldera complex, Nevada: Evidence for multiple cycles of chemical evolution in a long-lived silicic magma system: *Journal of Geophysical Research*, v. 94, p. 5961-5985.
- Carrigan, C. R., and Eichelberger, J. C., 1990, Zoning in magmas by viscosity in volcanic conduits: *Nature*, v. 343, p. 248-251.
- Druitt, T. H., and Sparks, R.S.J., 1984, On the formation of calderas during ignimbrite eruptions: *Nature*, v. 310, p. 679-681.
- Elston, W. E., 1984, Mid-Tertiary ash flow tuff cauldrons, southwestern New Mexico: *Journal of Geophysical Research*, v. 89, p. 8733-8750.
- Francis, P. W., Sparks, R.S.J., Hawkesworth, C. J., Thorpe, R. S., Pyle, D. M., Tait, S. R., Mantovani, M. S., and McDermott, F., 1989, Petrology and geochemistry of volcanic rocks of the Cerro Galan caldera, northwest Argentina: *Geological Magazine*, v. 126, p. 515-547.
- Fridrich, C. J., and Mahood, G. A., 1987, Compositional layers in a zoned magma chamber of the Grizzly Peak Tuff: *Geology*, v. 15, p. 299-303.
- Hartlow, F. H., and Amsden, A. A., 1975, Numerical calculation of multiphase fluid flow: *Journal of Computational Physics*, v. 17, p. 19-52.
- Heiken, G., Goff, F., Stix, J., Tamanyu, S., Shafiqullah, M., Garcia, S., and Hagan, R., 1986, Intracaldera volcanic activity, Toledo caldera and embayment, Jemez Mountains, New Mexico: *Journal of Geophysical Research*, v. 91, p. 1799-1815.
- Hildreth, W., 1981, Gradients in silicic magma chambers: Implications for lithospheric magmatism: *Journal of Geophysical Research*, v. 86, p. 10153-10192.
- Kieffer, S. W., and Sturtevant, B., 1988, Erosional furrows formed during the lateral blast at Mount St. Helens, May 18, 1980: *Journal of Geophysical Research*, v. 93, p. 14793-14816.
- Lipman, P. W., 1976, Caldera-collapse breccias in the western San Juan Mountains, Colorado: *Geological Society of America Bulletin*, v. 87, p. 1397-1410.
- , 1984, The roots of ash flow calderas in western North America: Windows into the tops of granitic batholiths: *Journal of Geophysical Research*, v. 89, p. 8801-8841.
- Marsh, B. D., 1989, Magma chambers: *Annual Reviews of Earth and Planetary Science*, v. 17, p. 439-474.
- Oldenburg, C. M., Spera, F. J., Yuen, D. A., and Sewell, G., 1989, Dynamic mixing in magma bodies: Theory, simulations, and implications: *Journal of Geophysical Research*, v. 94, p. 9215-9236.
- Rose, W. I., and Chesner, C. A., 1987, Dispersal of ash in the great Toba eruption, 75 ka: *Geology*, v. 15, p. 913-916.
- Self, S., Goff, F., Gardner, J. N., Wright, J. V., and Kite, W. M., 1986, Explosive rhyolitic volcanism in the Jemez Mountains: Vent locations, caldera development and relation to regional structure: *Journal of Geophysical Research*, v. 91, p. 1779-1798.
- Smith, R. L., 1960, Zones and zonal variations in welded ash flows: U.S. Geological Survey Professional Paper 354-F, 68 p.
- Smith, R. L., Bailey, R. A., and Ross, C. S., 1970, Geologic map of the Jemez Mountains, New Mexico: U.S. Geological Survey Map I-571.
- Sparks, R.S.J., 1976, Grain size variations in ignimbrites and implications for the transport of pyroclastic flows: *Sedimentology*, v. 23, p. 147-188.
- Sparks, R.S.J., Self, S., and Walker, G.P.L., 1973, Products of ignimbrite eruptions: *Geology*, v. 1, p. 115-118.
- Sparks, R.S.J., Wilson, L., and Hulme, G., 1978, Theoretical modeling of the generation, movement, and emplacement of pyroclastic flows by column collapse: *Journal of Geophysical Research*, v. 83, p. 1727-1739.
- Spera, F. J., Yuen, D. A., Greer, J. C., and Sewell, G., 1986, Dynamics of magma withdrawal from stratified magma chambers: *Geology*, v. 14, p. 723-726.
- Steven, T. A., and Lipman, P. W., 1976, Calderas of the San Juan volcanic field, southwestern Colorado: U.S. Geological Survey Professional Paper 958, 35 p.
- Triel, A. F., and Spera, F. J., 1990, Mechanisms for the generation of compositional heterogeneities in magma chambers: *Geological Society of America Bulletin*, v. 102, p. 353-367.
- Turner, J. S., 1973, Buoyancy effects in fluids: London, New York, Cambridge University Press, 367 p.
- Valentine, G. A., 1987, Stratified flow in pyroclastic surges: *Bulletin of Volcanology*, v. 49, p. 616-630.
- Valentine, G. A., and Wohletz, K. H., 1989a, Numerical models of Plinian eruption columns and pyroclastic flows: *Journal of Geophysical Research*, v. 94, p. 1867-1887.
- , 1989b, Environmental hazards of pyroclastic flows determined by numerical models: *Geology*, v. 7, p. 641-644.
- Warren, R. G., Byers, F. M., Jr., Broxton, D. E., Freeman, S. H., and Hagan, R. C., 1989, Phenocryst abundances and glass and phenocryst compositions, as indicators of magmatic environments of large-volume ash flow sheets in southwestern Nevada: *Journal of Geophysical Research*, v. 94, p. 5987-6020.
- Wilson, C.J.N., Rogan, A. M., Smith, I.E.M., Northey, D. J., Nairn, I. A., and Houghton, B. F., 1984, Caldera volcanoes of the Taupo volcanic zone, New Zealand: *Journal of Geophysical Research*, v. 89, p. 8463-8484.
- Wilson, L., Sparks, R.S.J., and Walker, G.P.L., 1980, Explosive volcanic eruptions; IV, The control of magma properties and conduit geometry on eruption column behavior: *Royal Astronomical Society Geophysical Journal*, v. 63, p. 117-148.
- Wohletz, K. H., and Valentine, G. A., 1990, Computer simulation of explosive volcanic eruptions, in Ryan, M., ed., *Magma storage and transport*: New York, John Wiley Publishing Co., p. 113-135.
- Wohletz, K. H., McGetchin, T. R., Sandford, M. T., II, and Jones, E. M., 1984, Hydrodynamic aspects of caldera-forming eruptions: Numerical experiments: *Journal of Geophysical Research*, v. 89, p. 8269-8286.
- Woods, A. W., 1988, The fluid dynamics and thermodynamics of eruption columns: *Bulletin of Volcanology*, v. 50, p. 169-193.

MANUSCRIPT RECEIVED BY THE SOCIETY DECEMBER 10, 1990
 REVISED MANUSCRIPT RECEIVED JULY 16, 1991
 MANUSCRIPT ACCEPTED JULY 29, 1991